ELSEVIER

International Journal of Mass Spectrometry 204 (2001) 7–21

International Journal of Mass Spectrometry

Determination of weak Fe^+–L bond energies (L = Ar, Kr, Xe, N_2, and CO_2) by ligand exchange reactions and collision-induced dissociation

Brenda L. Tjelta[1], Derek Walter[2], P.B. Armentrout*

Department of Chemistry, University of Utah, Salt Lake City, Utah 84112, USA

Received 7 February 2000; accepted 6 March 2000

Abstract

Guided-ion beam mass spectrometry is used to study the ligand exchange and collision induced dissociation reactions of $Fe^+(N_2)$ with Ar, Kr, Xe, CO_2, and CD_4 and $Fe^+(CO_2)$ with Kr, Xe, and N_2 as a function of kinetic energy. Analysis of the energy dependent cross sections provides threshold energies for both types of reactions. These thresholds can be converted to the following 0 K bond dissociation energies: $D_0(Fe^+–Ar) = 0.11 \pm 0.08$ eV, $D_0(Fe^+–Kr) = 0.31 \pm 0.07$ eV, $D_0(Fe^+–Xe) = 0.44 \pm 0.06$ eV, $D_0(Fe^+–N_2) = 0.55 \pm 0.04$ eV, and $D_0(Fe^+–CO_2) = 0.62 \pm 0.04$ eV. Our results are compared with experimental and theoretical values found in the literature. These comparisons suggest that $Fe^+(CO_2)$ has a linear structure in agreement with theoretical calculations. (Int J Mass Spectrom 204 (2001) 7–21) © 2001 Elsevier Science B.V.

Keywords: Bond energies; Iron; Rare gases; Collision-induced dissociation; Ligand exchange reactions

1. Introduction

In recent years, complexes of transition-metal cations M^+ with closed shell atoms have been studied extensively as some of the simplest possible examples of Lewis acid–base interactions. Although such complexes are held together largely through electrostatic forces, the open shell character of most transition metals leads to more complex interactions than might be expected naively. In addition to rare gas atoms, small inorganic molecules that are relatively inert can also act as weakly bound ligands for transition metal cations. For the more unusual N_2 and CO_2 ligands, there is the intriguing possibility that such complexes may act as precursors to the reformation of these molecules in nitrogen fixation chemistry and carbon dioxide activation. Characterization of such species has been achieved by theoretical means [1–7] and by experiments such as photodissociation spectroscopy [8–13], ion chromatography equilibria [14,15], and ligand exchange equilibria [16–18]. In the present work, we add guided ion beam mass spectrometry to the arsenal of techniques used to study these weakly bound transition metal complexes. By utilizing the kinetic energy dependence of ligand exchange reac-

* Corresponding author. E-mail: armentrout@chemistry.utah.edu

[1] Present address: Department of Chemistry, Siena College, Loudonville, NY, 12211.

[2] Present address: Department of Chemistry and Biochemistry, UCLA, Los Angeles, CA 90095.

PII S1387-3806(00)00342-0

tions, the relative binding affinities of various ligands can be ascertained and then anchored to an absolute scale by collision-induced dissociation (CID) measurements.

The present study is devoted to complexes of Fe^+, one of the transition-metal cations for which a large number of experimentally determined bond energies to neutral closed-shell ligands is known [19]. Of particular relevance to the present investigation are the studies conducted by Schwarz and co-workers [16–18]. In their earlier Fourier transform ion cyclotron resonance (FTICR) mass spectrometry work, Schwarz and Schwarz [16] found they could generate the weakly bound $Fe^+(CO_2)$ complex by reacting Fe^+ with β-butyrolactone. They then determined that Xe would displace the CO_2 ligand whereas Ar would not, thus bracketing $D_0(Fe^+–CO_2)$ between a theoretical value for $D(Fe^+–Ar) = 0.31$ eV [2] and an experimental value for $D(Fe^+–Xe) = 0.39 \pm 0.09$ eV, taken from work in our laboratory [20]. In a FTICR study devoted primarily to characterization of $Fe^+(N_2)$, Schwarz et al. refined this result by establishing that Kr also would not displace CO_2, whereas N_2 does [17]. In addition, the observation of ligand exchange reactions at thermal energies of $Fe^+(N_2)$ with C_2H_6, CH_4, and Xe and the failure to observe ligand displacement with Ar and Kr was used by Schwarz et al. [17] to determine relative bond dissociation energies (BDEs) for the FeL^+ species for L = Kr, Xe, and N_2. This study also included a theoretical characterization of the $Fe^+–N_2$ complex in terms of its electronic structure and bond energy. By measuring the forward and reverse rate constants for

$$Fe^+(N_2) + Xe \rightarrow FeXe^+ + N_2 \quad (1)$$

these authors used an equilibrium assumption to establish that the $Fe^+–N_2$ BDE is 0.074 ± 0.065 eV stronger than $D(Fe^+–Xe)$. An interesting aspect of this reaction is that at 298 K, reaction (1) is an entropically driven process because there are two more rotational degrees of freedom on the product side. In their most recent study of these systems, Schwarz et al. determined the relative bond energies of Fe^+ with Xe, N_2, CO_2, and CH_4 by examining several equilibria involving these complexes [18]. These relative values were anchored using $D_0(Fe^+–CH_4)$ determined by CID studies in our laboratory [21].

In the present study, we further investigate these weakly bound ligand exchange reactions. Here, direct measurements of the enthalpy associated with the ligand exchange reactions for $Fe^+(N_2)$ with Ar, Kr, Xe, CO_2, and CD_4 and $Fe^+(CO_2)$ with Kr, Xe, and N_2 are made. The entropy term for each reaction is also estimated so that these values can be converted to free energies of reaction, which can be compared directly with the results of Schwarz et al. [18]. We have previously determined the $Fe^+–N_2$ BDE by CID measurements with Xe to be 0.56 ± 0.06 eV [22]. Here, this value is refined using additional CID measurements and then used to determine the absolute BDEs of Fe^+–L species (L = Ar, Kr, Xe, CO_2). We also measure an independent ladder of values anchored to the $Fe^+–CO_2$ BDE determined by CID measurements. These values are compared to the Fe^+–rare gas species previously characterized by theory [5,6], to the Fe^+–Xe bond strength determined previously in our laboratory [20–23], and to the relative Fe^+–L bond energy scale established by Schwarz and co-workers [16–18]. Good agreement is found among all these independent determinations, except for the final bond enthalpy for the $Fe^+(CO_2)$ complex. The discrepancy for this complex results exclusively from differing assumptions regarding its molecular constants.

2. Experimental

2.1. General

The guided-ion beam instrument on which these experiments were performed has been described in detail previously [24,25]. Ions are created in a flow tube source as described in the following, extracted from the source, accelerated, and passed through a magnetic sector for mass analysis. The mass-selected ions are decelerated to the desired kinetic energy and focused into an octopole beam guide. This device uses

radio-frequency electric fields to trap the ions in the radial direction to insure complete collection of reactant and product ions [26,27]. The octopole passes through a gas cell that contains the neutral collision partner at a fairly low pressure. Studies performed at three different pressures (~0.05, 0.1, and 0.2 mTorr) demonstrate that none of the product cross sections exhibit any dependence on the pressure of the neutral reactant. The unreacted parent and product ions drift to the end of the octopole from which they are extracted, passed through a quadrupole mass filter for mass analysis, and detected with a secondary electron scintillation ion detector using standard pulse counting techniques. Raw ion intensities are converted to cross sections as described previously [24]. We estimate absolute cross sections to be accurate to ±20%.

Laboratory (lab) energies are converted to energies in the center-of-mass (CM) frame by using the conversion $E_{CM} = E_{lab}\ M/(M + m)$, where m and M are the ion and neutral reactant masses, respectively. The absolute energy scale and corresponding full width at half maximum (FWHM) of the ion beam kinetic energy distribution are determined using the octopole as a retarding energy analyzer as described previously [24]. The absolute uncertainty in the energy scale is ±0.05 eV (lab). The ion energy distributions are nearly Gaussian and have a typical FWHM of 0.2–0.5 eV (lab).

2.2. Ion source

The metal–ligand ions are formed in a 1 m long flow tube [25] operating at a pressure of 0.4–0.7 Torr with a helium flow rate of 4000–9000 standard cm^3/min. Fe^+ is produced by argon ion sputtering of an iron cathode in a flow of 5%–10% argon in helium. The reactant ions $Fe^+(L)$ where $L = N_2$ or CO_2 are formed by three-body associative reactions of Fe^+ with N_2 or CO_2 molecules. The ligand gas is added 50 cm downstream from the dc discharge and was less than 10% of the total flow.

The flow conditions used in the flow tube ion source provide approximately 10^5 collisions between an ion and the buffer gas, which should thermalize the ions both rotationally and vibrationally. We assume that the internal energy of the ions produced in this source is well described by a Maxwell-Boltzmann distribution of rotational and vibrational states corresponding to 298 K. Previous work from this laboratory has shown that this assumption is valid [20,28–30].

2.3. Thermochemical analysis

Theory and experiment [31,32] have shown that endothermic cross sections can be modeled in the threshold region with

$$\sigma(E) = \sigma_0 \sum g_i(E + E_{rot} + E_{vib} + E_i - E_0)^n/E \quad (2)$$

where σ_0 is an energy independent scaling factor, E is the relative translational energy of the reactants, E_{rot} is the average rotational energy of the reactants [kT = 0.026 eV for $Fe^+(L)$ + Xe, Kr, Ar; $2kT$ = 0.052 eV for $Fe^+(L)$ + N_2, CO_2; $5kT/2$ = 0.064 eV for $Fe^+(L)$ + CD_4], E_{vib} is the vibrational energy of the neutral reactant (negligible for N_2, 0.004 eV for CD_4, and 0.008 eV for CO_2 at 300 K as calculated using vibrational frequencies from Shimanouchi [33]), E_0 is the threshold for reaction of the ground vibrational and electronic state, and n is an adjustable parameter. The internal energy of the $Fe^+(L)$ reactant ion is included explicitly as a summation over vibrational energy levels, i, with energies E_i and relative populations $g_i(\Sigma g_i = 1)$. We assume that the relative reactivity, as reflected by σ_0 and n, is the same for all vibrational states. We use the Beyer-Swinehart [34–37] algorithm to calculate a Maxwell-Boltzmann distribution of vibrational energies at 298 K, which is used for the factors g_i in Eq. (2).

At higher energies, some of the cross sections peak and then decline. To model this behavior, we use a modified form of Eq. (2) that accounts for a decline in the product ion cross section at higher kinetic energies. This model has been described in detail previously [38] and depends on E_D, the energy at which a dissociation channel can begin, and p, a parameter similar to n in Eq. (2).

Because the vibrational, rotational, and translational energy distributions of the reactants are explic-

Table 1
Electronic ground states, rotational constants, vibrational frequencies, and entropies of iron ligand cation complexes

Species	State	B (cm^{-1})	Frequency (cm^{-1})[a]	S(J/mol K)
$FeAr^+$	$^6\Delta$[b]	0.092[c]	98[b]	273.6
	$^4\Phi$[b]	0.119[c]	157[b]	264.2
$FeKr^+$	$^4\Phi$[b]	0.078[c]	149[b]	272.9
$FeXe^+$	$^4\Phi$[b]	0.062[c]	159[b]	277.9
$Fe^+(N_2)$	$^4\Sigma^-$[d]	0.135[e]	275 (2), 318, 2358[d]	263.6
$Fe^+(CO_2)$ Linear	$^6\Delta$[f]	0.054[g]	213,[f] 263 (2), 667 (2), 1385, 2349[g]	285.6
$Fe^+(CO_2)$ Nonlinear	^6A[f]	0.123, 0.179, 0.390[g]	129, 186, 667 (2), 1385, 2349[g]	299.7
$Fe^+(CH_4)$	$^4A_2$[h]	0.284 (2), 5.278[i]	353 (2), 409, 1306 (3), 1534 (2), 2916, 3019 (3)[g]	265.8
$Fe^+(CD_4)$	$^4A_2$[h]	0.231 (2), 2.642[i]	325 (2), 376, 996 (3), 1092 (2), 2109, 2259 (3)[g]	274.9

[a] Degeneracies in parentheses.
[b] See [6].
[c] Calculated using bond distances from [6].
[d] See [17].
[e] Calculated using bond distances from [17].
[f] See [7].
[g] Frequencies estimated as outlined in the text.
[h] See [46].
[i] Calculated using bond distances from [46].

itly included in our modeling, threshold values correspond to 0 K values. We take the 0 K thresholds to equal the endothermicities of reaction, which assumes that there are no activation barriers to these processes in excess of the endothermicities. This assumption is generally true for ion-molecule reactions [32,39–42] and should be valid for the simple bond fission and exchange reactions studied here [43].

2.4. Molecular constants

Molecular constants for all reactants and product complexes are listed in Table 1 and determined as follows. For Fe^+–L (L = Ar, Kr, Xe), rotational constants were calculated using the bond distances reported in [6], and for $Fe^+(N_2)$, in [17]. Vibrational frequencies were also taken from these references. These studies have also determined that $FeKr^+$, $FeXe^+$, and $Fe^+(N_2)$ have quartet ground states. The quartet and sextet states of $FeAr^+$ are close enough in energy that the ground state cannot be definitively assigned. Therefore we consider both possibilities explicitly.

For a linear $Fe^+(CO_2)$ complex, the rotational constants are calculated using the geometry calculated by Sodupe et al. [7]. Vibrational frequencies of this complex are assumed to equal those of free CO_2 [44] along with an Fe–ligand stretch from theory, 213 cm^{-1} [7]. The bends are obtained by scaling the analogous $Fe^+(N_2)$ frequencies [17] according to a Morse potential. Thus, the frequencies are proportional to $(D_e/\mu)^{1/2}$, where D_e and μ are the equilibrium bond energy and reduced mass, respectively. With this approximation, the ratio of the Fe^+–N_2 to Fe^+–CO_2 frequencies, $\omega_1/\omega_2 = [(D_e/\mu)_1/(D_e/\mu)_2]^{1/2} \approx 1.05$. For completeness, we also consider a nonlinear $Fe^+(CO_2)$ structure (T-shaped geometry), where the rotational constants are estimated as that for free CO_2 [44] and those calculated using an Fe^+–C bond distance equal to Fe^+–N_2 [17]. For the vibrational frequencies of nonlinear $Fe^+(CO_2)$, the frequencies calculated for $Fe^+(CS_2)$ [45] were scaled by 0.6 (on the basis of a Morse potential) and are used in conjunction with the frequencies for free CO_2 [44]. Sodupe et al. [7] calculated that linear $Fe^+(CO_2)$ has a $^6\Delta$ ground state with low-lying $^6\Pi$ and $^4\Phi$ excited states. For nonlinear $Fe^+(CO_2)$ having C_{2v} symmetry, we do not differentiate among several possible ground

Table 2
Summary of fitting parameters used in Eq. (2)

Reactants	Products	E_0 (eV)	σ_0	n
$Fe^+(N_2)$ + Ar	$FeAr^+ + N_2$	$0.43_8 \pm 0.08$	0.4 ± 0.1	0.8 ± 0.3
	$Fe^+ + Ar + N_2$	$0.54_2 \pm 0.05$	8.0 ± 0.6	1.7 ± 0.2
$Fe^+(N_2)$ + Kr	$FeKr^+ + N_2$	$0.17_6 \pm 0.06$	1.1 ± 0.3	1.4 ± 0.2
	$Fe^+Kr + N_2$	$0.54_4 \pm 0.06$	7.0 ± 0.7	1.8 ± 0.2
$Fe^+(N_2)$ + Xe	$FeXe^+ + N_2$	$0.09_4 \pm 0.06$	3.2 ± 1.3	0.5[a]
	$Fe^+ + Xe + N_2$	0.56 ± 0.06[b]	8.7 ± 2.7[b]	1.6 ± 0.2[b]
$Fe^+(N_2)$ + CO_2	$Fe^+(CO_2) + N_2$	<0		
	$Fe^+ + CO_2 + N_2$	0.51 ± 0.05	8.3 ± 0.7	1.5 ± 0.3
$Fe^+(N_2)$ + CD_4	$Fe^+(CD_4) + N_2$	<0		
$Fe^+(CO_2)$ + Kr	$FeKr^+ + CO_2$	$0.33_4 \pm 0.03_5$	3.7 ± 0.3	1.8 ± 0.1
	$Fe^+ + Kr + CO_2$	$0.65_5 \pm 0.04_6$	11.4 ± 0.5	1.2 ± 0.2
$Fe^+(CO_2)$ + Xe	$FeXe^+ + CO_2$	$0.15_8 \pm 0.04_1$	1.6 ± 0.2	0.4 ± 0.1
	$Fe^+ + Xe + CO_2$	$0.65_8 \pm 0.04_7$	18.8 ± 1.6	1.2 ± 0.2
$Fe^+(CO_2)$ + N_2	$Fe^+(N_2) + CO_2$	$0.09_2 \pm 0.03_2$	2.8 ± 0.5	0.3 ± 0.1
	$Fe^+ + N_2 + CO_2$	$0.59_6 \pm 0.04_5$	11.4 ± 0.5	1.2 ± 0.2

[a] This parameter was held constant and not optimized.
[b] See [22].

states other than to signify that the orbital degeneracy is unity.

For $Fe^+(CH_4)$ and $Fe^+(CD_4)$, we use the frequencies of the free ligands [33] along with metal–ligand frequencies scaled from $Fe^+(N_2)$ according to the Morse potential analysis (ratios of 0.78 and 0.85, respectively). The rotational constants are determined using geometries calculated by Ricca et al. [46] for the ground state having an η^3 coordination and quartet spin. Uncertainties in the rotational constants are derived using assumed uncertainties of 10% in the bond distances.

We estimate the sensitivity of our analysis to uncertainties in these frequencies as described in our work on $H_3O^+(H_2O)_x$(x = 1–5) [29] and $M^+(H_2O)_x$ (M = Ti–Cu, x = 1–4) [30]. All of the vibrational frequencies except for the internal modes of the ligands were scaled by ±25%, and the corresponding change in the average vibrational energy is taken to be an estimate of one standard deviation of the uncertainty in vibrational energy.

3. Results

For all reactions studied here, the only processes observed were loss of intact nitrogen or carbon dioxide ligands in ligand exchange processes and collision-induced dissociation (CID),

$$Fe^+(L) + Rg \rightarrow FeRg^+ + L \quad (3)$$

$$\rightarrow Fe^+ + L + Rg \quad (4)$$

where L = N_2 or CO_2 and Rg = Ar, Kr, Xe, N_2, CO_2, or CD_4. In all systems, the cross sections for both reactions are analyzed using Eq. (2) and yield the optimized parameters listed in Table 2.

Because of the very high BDE of the dinitrogen triple bond (D_0 = 9.90 eV [47]), it is highly unlikely that the transition-metal ion can insert to generate $NFeN^+$. In contrast, the sum of the FeO^+ (D_0 = 3.47 ± 0.05 eV [19]) and $Fe^+(CO)$ (D_0 = 1.59 ± 0.08 eV [20,22]) bond energies mean that insertion of Fe^+ into a carbon–oxygen double bond (D_0 = 5.453 ± 0.002 eV [48]) to form $OFeCO^+$ is thermodynamically feasible. However, when either $Fe^+(N_2)$ and $Fe^+(CO_2)$ are mass selected and subjected to collisional activation with any reactant gas, the complex decomposes exclusively to Fe^+ and L over the entire energy regime studied (CM energies cover a range of 0–30 eV). No FeO^+ products are observed at higher collision energies, discounting the

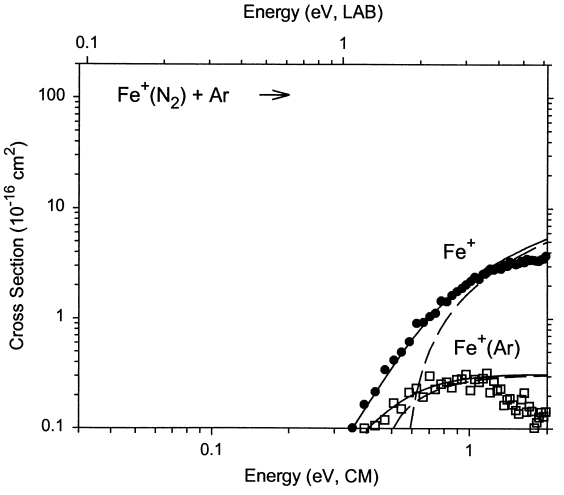

Fig. 1. Cross sections for reaction of $Fe(N_2)^+$ and argon as a function of kinetic energy in the center-of-mass frame (lower scale) and laboratory frame (upper scale). The solid lines are the best fits of Eq. (2) convoluted over the neutral and ionic kinetic energy distribution. The unconvoluted models for 0 K reactants are shown as the dashed lines.

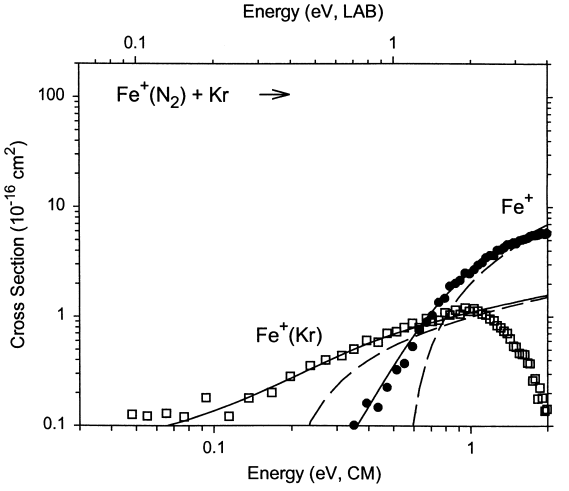

Fig. 2. Cross sections for reaction of $Fe(N_2)^+$ and krypton as a function of kinetic energy in the center-of-mass frame (lower scale) and laboratory frame (upper scale). The solid lines are the best fits of Eq. (2) convoluted over the neutral and ionic kinetic energy distribution. The unconvoluted models for 0 K reactants are shown as the dashed lines.

possibility that the $Fe^+(CO_2)$ reactant ions have the $OFeCO^+$ structure.

3.1. $Fe^+(N_2)$ + Rg

Results for the interaction of $Fe^+(N_2)$ with Ar, Kr, Xe, CO_2, and CD_4 are shown in Figs. 1–5. In the case of Ar, both CID and ligand exchange are endothermic processes that rise from similar apparent thresholds near ~0.3 eV. The major product channel at all energies is the CID process to form Fe^+ which rises to a maximum cross section magnitude of ~4 Å^2, over an order of magnitude larger than the $FeAr^+$ product cross section. The $FeAr^+$ cross section reaches a maximum at higher energies, indicating that this product begins to dissociate to form Fe^+. Such high energy behavior is observed for all ligand exchange reactions studied here.

For the interaction of $Fe^+(N_2)$ with Kr, the ligand exchange product cross section has a threshold that is clearly lower in energy than the CID product cross section. In this case, the $FeKr^+$ product cross section rises from a threshold near 0.1 eV to a maximum

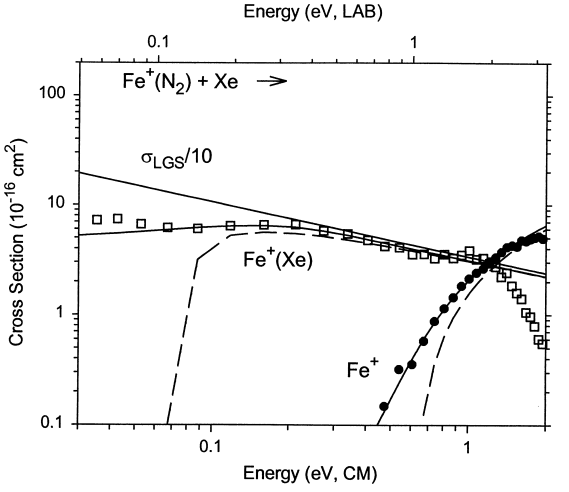

Fig. 3. Cross sections for reaction of $Fe(N_2)^+$ and xenon as a function of kinetic energy in the center-of-mass frame (lower scale) and laboratory frame (upper scale). The solid lines are the best fits of Eq. (2) convoluted over the neutral and ionic kinetic energy distribution. The unconvoluted models for 0 K reactants are shown as the dashed lines. Also shown as a solid line is the collision cross section, σ_{LGS}, divided by 10.

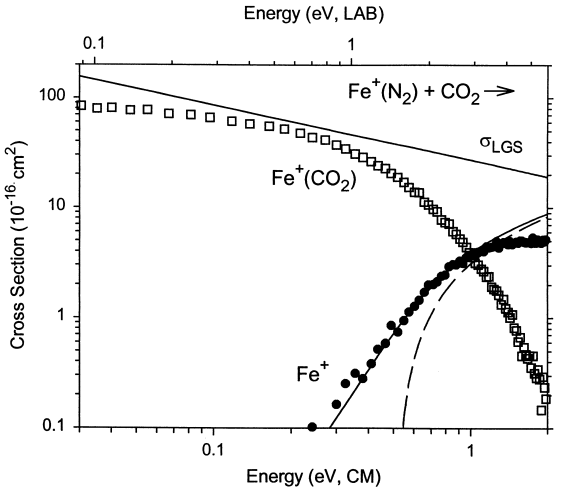

Fig. 4. Cross sections for reaction of $Fe(N_2)^+$ and carbon dioxide as a function of kinetic energy in the center-of-mass frame (lower scale) and laboratory frame (upper scale). The solid line is the best fit of Eq. (2) convoluted over the neutral and ionic kinetic energy distribution. The unconvoluted model for 0 K reactants is shown as the dashed line. Also shown as a solid line is the collision cross section, σ_{LGS}.

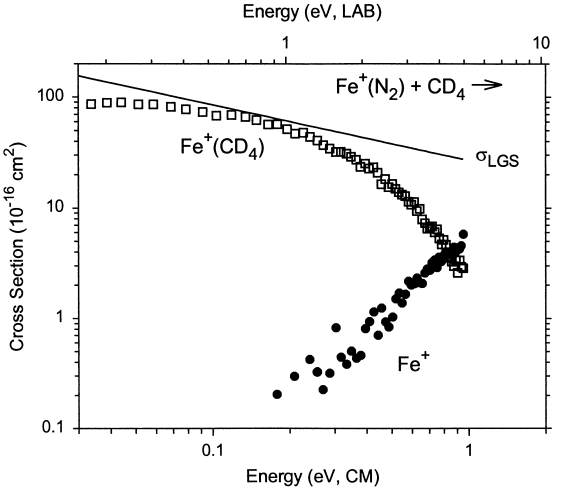

Fig. 5. Cross sections for the reaction of $Fe(N_2)^+$ with CD_4 as a function of kinetic energy in the center-of-mass frame (lower scale) and laboratory frame (upper scale). Also shown as a solid line is the collision cross section, σ_{LGS}.

cross section slightly larger than 1 Å^2 at 1 eV. Threshold analysis of this cross section yields the expected result that the energy threshold for ligand exchange is considerably smaller than in the argon case. The Fe^+ cross sections are similar in the Ar and Kr systems, Figs. 1 and 2, as documented by comparable threshold analyses, Table 2.

For the interaction of $Fe^+(N_2)$ with Xe, CO_2, and CD_4, the ligand exchange processes exhibit finite cross sections at the lowest energies, Figs. 3–5. In all three systems, these cross sections increase with decreasing energy, an energy dependence generally attributed to a barrierless, exothermic process. The $FeXe^+$ cross section has a maximum cross section magnitude of ~7 Å^2 below 0.2 eV. The $Fe^+(CO_2)$ and $Fe^+(CD_4)$ cross sections are nearly identical and about an order of magnitude larger than $FeXe^+$. A more quantitative analysis of these cross sections can be obtained by a detailed comparison to the Langevin-Gioumousis-Stevenson (LGS) model for ion-molecule collisions [49]. The LGS model for the collision cross section of an ion–molecule reaction at low energies is given by $\sigma_{LGS} = \pi e(2\alpha/E)^{1/2}$, where e is the electron charge, α is the polarizability of the target molecule, and E is the relative kinetic energy of the reactants. The polarizabilities are obtained from [50].

The observed $FeXe^+$ cross section follows the predicted $E^{-1/2}$ energy dependence from 0.2 to 1.0 eV, but the magnitude is only 10 ± 6% of this prediction. The inefficiency of this process could be a result of kinetic or thermodynamic factors. The former seems improbable given the efficiencies of the analogous reactions with CO_2 and CD_4. Thermodynamic factors are a plausible explanation as this cross section can be reproduced throughout the low energy range using Eq. (2) while holding $n = 0.5$, as predicted for slightly endothermic ion–molecule reactions [51]. The optimized parameters obtained are given in Table 2. The observed $Fe^+(CO_2)$ and $Fe^+(CD_4)$ cross sections are close to the σ_{LGS} cross section in magnitude at the lowest energies, but differ somewhat from the predictions of σ_{LGS} in energy dependence at the lowest energies. These deviances could be an indication that these reactions are slightly endothermic, but such a conclusion would be inconsistent with the large magnitude of these cross sections. Rather we attribute these small deviations from

σ_{LGS} primarily to the absolute uncertainties in the energies, which are 0.017 and 0.010 eV, respectively.

In both the Xe and CO_2 cases, the CID processes to form Fe^+ rise from similar thresholds (Table 2) to cross-section maxima of ~6 Å^2. The cross-section magnitudes for the CID process are similar to those for the Kr and Ar collision gases and similar thresholds are obtained, Table 2. However, the apparent threshold in the rare gas systems is higher than in the CO_2 system (Figs. 1–3 versus 4), illustrating the higher energy content of the neutral reagents in the latter system and a slightly lower E_0 value. The observation that the E_0 values agree within experimental uncertainty in all cases shows that competition with the lower energy ligand exchange process does not influence the threshold for the CID process. In the reaction with CD_4, the CID process was not analyzed in detail because the cross section is much noisier than for the other systems. The poor quality is because these data were acquired simply to ascertain the relative energetics of the N_2 and CD_4 ligands by examining the ligand exchange process.

3.2. $Fe^+(CO_2)$ + Rg

Results for the interaction of $Fe^+(CO_2)$ with Kr, Xe, and N_2 are shown in Figs. 6–8. For the interaction of $Fe^+(CO_2)$ with Kr, the ligand exchange cross section has a threshold that is clearly lower in energy than the CID product cross section. In this case, the $FeKr^+$ product cross section rises from a threshold near 0.2 eV to a maximum cross section of less than 1 Å^2 at 0.7 eV. For the interaction of $Fe^+(CO_2)$ with Xe and N_2, the ligand exchange processes exhibit finite cross sections at low energies, Figs. 7 and 8. The $FeXe^+$ cross section has a maximum cross section magnitude of ~4 Å^2 at 0.2 eV, and falls slightly as energy is decreased further. In contrast, the $Fe^+(N_2)$ cross section increases monotonically with decreasing energy. Compared with σ_{LGS}, the $FeXe^+$ cross section is about 6 ± 1% between 0.3 and 0.6 eV, whereas the $Fe^+(N_2)$ cross section is about 16 ± 3% below 0.3 eV. Clearly, the ligand exchange reaction of $Fe^+(CO_2)$ with Xe is endothermic, as verified by the threshold analysis, Table 2, which reproduces the

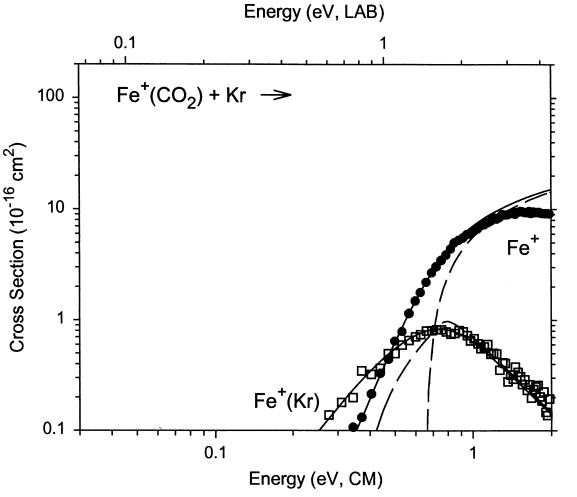

Fig. 6. Cross sections for reaction of $Fe(CO_2)^+$ and krypton as a function of kinetic energy in the center-of-mass frame (lower scale) and laboratory frame (upper scale). The solid lines are the best fits of Eq. (2) convoluted over the neutral and ionic kinetic energy distribution. The unconvoluted models for 0 K reactants are shown as the dashed lines.

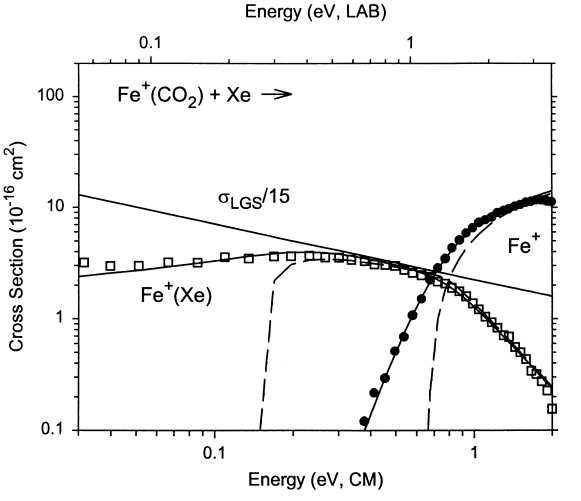

Fig. 7. Cross sections for reaction of $Fe(CO_2)^+$ and xenon as a function of kinetic energy in the center-of-mass frame (lower scale) and laboratory frame (upper scale). The solid lines are the best fits of Eq. (2) convoluted over the neutral and ionic kinetic energy distribution. The unconvoluted models for 0 K reactants are shown as the dashed lines. Also shown as a solid line is the collision cross section, σ_{LGS}, divided by 15.

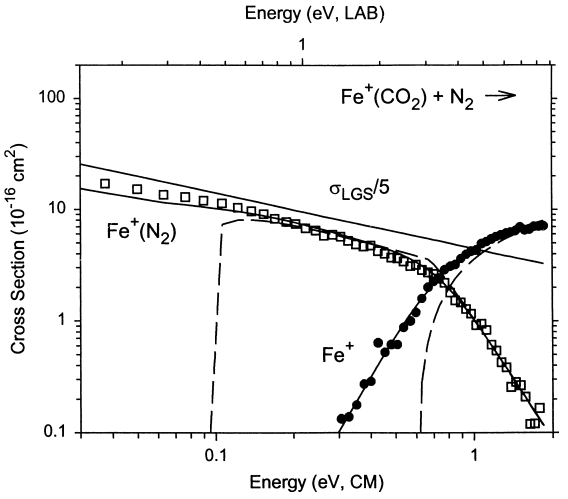

Fig. 8. Cross sections for reaction of $Fe(CO_2)^+$ and nitrogen as a function of kinetic energy in the center-of-mass frame (lower scale) and laboratory frame (upper scale). The solid lines are the best fits of Eq. (2) convoluted over the neutral and ionic kinetic energy distribution. The unconvoluted models for 0 K reactants are shown as the dashed lines. Also shown as a solid line is the collision cross section, σ_{LGS}, divided by 5.

$FeXe^+$ cross section throughout the low energy region, Fig. 7. Interestingly, the $Fe^+(N_2)$ cross section can also be reproduced using Eq. (2), Fig. 8. The optimized parameters are listed in Table 2, although it is not unambiguous that this process is endothermic. This ambiguity is discussed further in the following.

The CID processes of $Fe^+(CO_2)$ with Kr, Xe, and N_2 to form Fe^+ rise from apparent thresholds of 0.3–0.4 eV to cross section maxima of ~11 Å^2 for Kr and Xe and ~7 Å^2 for N_2. The threshold analyses of these three CID cross sections are similar, Table 2.

It is also informative to directly compare the cross sections for interaction of $Fe^+(N_2)$ and $Fe^+(CO_2)$ with Kr and Xe, Figs. 2 versus 6 and 3 versus 7. Comparison of the cross sections for the ligand exchange reactions clearly indicates lower thresholds in the $Fe^+(N_2)$ systems. This comparison is a direct indication that the $Fe^+(CO_2)$ bond energy is larger than that of $Fe^+(N_2)$. In apparent contrast, comparison of the CID cross sections finds similar apparent thresholds, however, this appearance can be attributed to the logarithmic scale used to display the data coupled with the larger cross section magnitudes for the dissociation of $Fe^+(CO_2)$.

3.3. CID threshold energies

In a previous study of the sequential bond energies of $Fe^+(N_2)_x$ (x = 1–5) [22], we reported our analysis of the threshold for the CID process, reaction (4), in the Xe system. This analysis yields a threshold of 0.56 ± 0.06 eV. In the present study, collisions of $Fe^+(N_2)$ with Ar, Kr, and CO_2 yield CID thresholds of 0.54 ± 0.05, 0.54 ± 0.06, and 0.51 ± 0.05 eV, respectively, Table 2. All these values are in excellent agreement with each other and the weighted average of our four experimental determinations is 0.54 ± 0.03 eV (where the uncertainty is one standard deviation).

The three collision gases used in the $Fe^+(CO_2)$ system yield thresholds for the CID process of 0.66 ± 0.05, 0.66 ± 0.05, and 0.60 ± 0.05 eV for Kr, Xe, and N_2, respectively, Table 2. Again the values are in good agreement with each other and yield a weighted average of 0.64 ± 0.03 eV (where the uncertainty is one standard deviation).

3.4. Relative Fe^+–Rg bond dissociation energies

The threshold energy for the ligand exchange channel, reaction (3), is the difference between the bond energies of L and Rg to Fe^+, namely,

$$E_0(FeRg^+) = D_0(Fe^+–L) - D_0(Fe^+–Rg) \quad (5)$$

Using this equation and the $D_0(Fe^+–L)$ values obtained by CID, the thresholds in Table 2 are converted to the relative bond energies shown in Table 3. Note that there is excellent agreement between the values for $D_0(Fe^+–N_2)$ obtained directly from CID measurements and relative to the $D_0(Fe^+–CO_2)$ bond energy. Further, the values obtained for $D_0(Fe^+–Xe)$ relative to the N_2 and CO_2 ligands agree nicely within the experimental errors. These values are slightly larger than those determined previously in our laboratory relative to CO [20] and H_2O [21] ligands, but are still within the experimental errors. The two values ob-

Table 3
Summary of CID and relative results for $D_0(Fe^+–L)$ in eV

L	CID (with X)[a]	Relative (X)[b]	Average[c]
Ar		0.11 ± 0.08 (N_2)	0.11 ± 0.08
Kr		0.37 ± 0.06 (N_2)	0.31 ± 0.07
		0.29 ± 0.04 (CO_2)	
Xe		0.45 ± 0.06 (N_2)[d]	0.44 ± 0.06
		0.47 ± 0.05 (CO_2)	
		0.39 ± 0.06 (H_2O)	
		0.39 ± 0.09 (CO)	
N_2	0.54 ± 0.05 (Ar)	0.54 ± 0.04 (CO_2)	0.54 ± 0.05 (CID)
	0.54 ± 0.06 (Kr)	0.59 ± 0.04 (Eq w CO_2)[e]	0.55 ± 0.04 (all)
	0.56 ± 0.06 (Xe)[d]		
	0.51 ± 0.05 (CO_2)		
CH_4	0.59 ± 0.03 (Xe)[f]	>0.54 ± 0.03 (N_2)	0.59 ± 0.06
CO_2	0.65 ± 0.05 (Kr)	0.63 ± 0.04 (N_2)	0.64 ± 0.05 (CID)
	0.66 ± 0.05 (Xe)	0.58 ± 0.04 (Eq w N_2)[e]	0.62 ± 0.04 (all)
	0.60 ± 0.05 (N_2)		

[a] Collision-induced dissociation threshold with indicated gas X.
[b] Calculated using the relative thresholds for ligand exchange reactions with gas X.
[c] Weighted mean of the indicated values. Uncertainties are two standard deviations of the mean, except for $FeAr^+$.
[d] See [22].
[e] Calculated from equilibrium assumption. See text.
[f] See [21].

tained for $D_0(Fe^+–Kr)$ relative to the N_2 and CO_2 ligands also agree within experimental uncertainty. Unsurprisingly, the Fe^+–Ar interaction is the weakest of the series at 0.11 ± 0.08 eV. Finally, the observation that CO_2 and CD_4 exothermically displace N_2 is consistent with the average bond energies in Table 3.

We can also obtain a relative value for the $Fe^+(N_2)$ and $Fe^+(CO_2)$ complexes by using the relative rate constants for the forward and backward reaction

$$Fe^+(N_2) + CO_2 \leftrightarrow Fe^+(CO_2) + N_2 \quad (6)$$

From the data in Figs. 4 and 8, we find that the ratio of the cross sections (forward/backward) at low energies is fairly constant, $\sigma_f/\sigma_b = 6 \pm 2$. We then calculate the equilibrium constant from $K_{eq} = k_f/k_b = (\sigma\nu)_f/(\sigma\nu)_b = (\sigma/\mu^{1/2})_f/(\sigma/\mu^{1/2})_b$ where $\nu = (2E/\mu)^{1/2}$, $\mu_f = 28.9$ u and $\mu_b = 21.9$ u. This equation yields $K_{eq} = 5.2 \pm 1.7$, from which $\Delta G_{298} = -RT \ln K_{eq} = -0.042 \pm 0.010$ eV can be obtained. These values are in good agreement with the determinations of Dieterle et al.: $K_{eq} = 3.8 \pm 0.8$ and $\Delta G_{298} = -0.035 \pm 0.009$ eV [18].

3.5. Conversion between 298 and 0 K thermochemistry

Further comparison of free energies of reaction with our other thermodynamic results requires conversion between 298 and 0 K thermochemistry. Given the molecular constants in Table 1, these quantities are straightforwardly calculated using standard formulae. Entropies of the iron cation complexes are listed in Table 1 and converted to entropies of reaction at 298 K, $T\Delta_r S_{298}$, listed in Table 4. The main uncertainties in the calculated entropies concern contributions from low-lying excited electronic states (which are ignored here) and the harmonic oscillator treatment of low-lying vibrational frequencies (which might be better treated as hindered rotors). Thus, we estimate uncertainties in these entropies at about ±10 J/mol K. The difference between the reaction enthalpies at 298 and 0 K, $\Delta_r H_{298} - \Delta_r H_0$, are also listed in Table 4. These can be combined to yield the listed $\Delta_r G_{298} - \Delta_r H_0$ values that have an uncertainty of about 0.03 eV. These correction terms can be com-

Table 4
Calculated thermodynamic functions for $Fe^+(L) + Rg \rightarrow Fe^+(Rg) + L$[a]

Rg	$T\Delta_rS_{298}$[b]	$\Delta_rH_{298} - \Delta_rH_0$[b]	$\Delta_rG_{298} - \Delta_rH_0$	Δ_rH_0[c]	Δ_rH_{298}	Δ_rG_{298}	Δ_rG_{298} (lit)[d]
$L = N_2$							
Ar	0.144	0.010	−0.134	0.44 (0.08)	0.45	0.30 (0.09)	
	0.115	0.007	−0.108	0.44 (0.08)	0.45	0.33 (0.09)	
Kr	0.114	0.008	−0.106	0.23 (0.08)	0.24	0.13 (0.08)	
Xe	0.112	0.007	−0.104	**0.11 (0.07)**	**0.12**	**0.01 (0.08)**	**−0.01 (0.01)**
CH_4	0.023	−0.008	−0.031	−0.04 (0.07)	−0.05	−0.07 (0.08)	−0.04 (0.01)
CD_4	0.009	−0.005	−0.014	−0.04 (0.07)	−0.05	−0.06 (0.08)	
$L = CO_2$ (linear)							
Kr	0.103	0.003	−0.100	0.31 (0.08)	0.31	0.21 (0.08)	
Xe	0.102	0.003	−0.099	0.19 (0.07)	0.19	0.09 (0.08)	0.03 (0.03)
N_2	0.010	−0.005	−0.015	0.08 (0.05)	0.07	0.06 (0.06)	0.03 (0.02)
				0.06 (0.03)[e]	0.05	0.04 (0.01)[e]	
CH_4	0.013	−0.013	−0.026	**0.03 (0.07)**	**0.02**	**0.01 (0.08)**	**−0.01 (0.01)**
$L = CO_2$ (nonlinear)							
Kr	0.071	−0.004	−0.075	0.31 (0.08)	0.31	0.24 (0.06)	
Xe	0.069	−0.004	−0.073	0.19 (0.07)	0.18	0.11 (0.08)	0.03 (0.02)
N_2	−0.043	−0.012	0.031	0.08 (0.05)	0.06	0.11 (0.06)	0.03 (0.01)
				0.01 (0.03)[e]	0.00	0.04 (0.01)[e]	
CH_4	−0.020	−0.020	0.000	0.03 (0.07)	0.01	0.03 (0.08)	−0.01 (0.01)

[a] All values in eV. All uncertainties are two standard deviations. Entries in bold face type indicate reactions where the free energy may change sign from 0 to 298 K.
[b] Calculated using molecular parameters given in Table 1. See text.
[c] Calculated from average values in Table 3 except as noted.
[d] See [18].
[e] Δ_rG_{298} value from ratio of forward and reverse cross sections for reaction (6), see text.

pared with those calculated by Schwarz and coworkers. For reaction (1), we find precisely the same adjustments as listed in detail by Schwarz et al. [17] for translation, rotation, and vibration. However, on the basis of the electronic states shown in Table 1, we include an electronic contribution to the entropy of reaction. Dieterle et al. [18] provide $\Delta_rG_{298} - \Delta_rH_0$ values for five processes, including reaction (1), but do not provide the molecular constants used that allow a detailed evaluation of these values. Our calculated adjustments agree nicely (within 0.005 eV given the difference in the electronic entropy term noted above) for the two reactions not involving CO_2. If a linear $Fe^+(CO_2)$ complex is assumed, our $\Delta_rG_{298} - \Delta_rH_0$ values lie an average of 0.060 eV lower than those listed by Dieterle et al. In contrast, an assumption of a T-shaped complex leads to values only 0.027 eV lower, within the errors of either work. Therefore, it appears that Dieterle et al. assumed molecular constants for $Fe^+(CO_2)$ that differ appreciably from those chosen here.

4. Discussion

4.1. Comparison with theoretical values

Table 5 compares our measured values with those from several theoretical studies [5,6,7,17,46,52]. Although the theoretical methods used in these studies vary, all calculations reported involve multireference configurations and have been corrected to 0 K values when necessary. It can be seen that the theoretical bond energies for the quartet ground states of $Fe^+(N_2)$ [17] and $Fe^+(CH_4)$ [46] agree well with our experimental values as determined by CID. Theoretical values for the low-lying sextet states are substantially lower, although the differences may be within the combined errors of experiment and theory. If our CID measurements corresponded to spin-allowed dissociation of the FeL^+ (^4X) complexes to $Fe^+(^4F)$ + L, then the adiabatic experimental bond energies would be lower than the CID thresholds by the ^6D–^4F excitation energy of 0.23 eV [53], in much worse

Table 5
Comparison of literature and present values for $D_0(Fe^+–L)$ in eV[a]

L	This work	Previous experiment[b]	Theory	State
Ar	0.11 ± 0.08		0.245 ± 0.1,[c] 0.137[d]	$^6\Delta$
			0.250 ± 0.1,[c] 0.081[d]	$^4\Phi$
Kr	0.31 ± 0.07		0.415 ± 0.1[c]	$^4\Phi$
Xe	0.44 ± 0.06	0.51 ± 0.07	0.615 ± 0.1[c]	$^4\Phi$
		[0.48 ± 0.08][e]		
N_2	0.55 ± 0.04	0.58 ± 0.07	0.52 ± 0.10[f]	$^4\Sigma^-$
			0.38	$^6\Delta$
CH_4	0.59 ± 0.06	0.59 ± 0.06	0.59,[g] 0.60[h]	$^4A_2$
			0.43,[g] 0.39[h]	$^6A_2$
CO_2	0.62 ± 0.04	0.56 ± 0.08	0.70[i]	$^6\Delta$
		[0.63 ± 0.08][e]	0.64[i]	$^4\Phi$

[a] All values calculated with respect to $Fe^+(^6D)$ + L asymptote. All uncertainties are two standard deviations.
[b] See [18].
[c] See [6].
[d] Calculated value for the $^4\Phi$ state has been adjusted for the experimental $^4F–^6D$ splitting of Fe^+. See [5].
[e] Value recalculated using $\Delta_r G_{298} - \Delta_r H_0$ from Table 4.
[f] See [17].
[g] See [46].
[h] See [52].
[i] See [7].

agreement with theory for the quartet state. (Although these lower numbers would agree well with the theoretical values for the sextet states, this assignment belies the underlying assumption used to derive these lower experimental values that the complexes have quartet ground states.) Although not definitive, it seems fairly certain that our experimental bond energies correspond to quartet ground states dissociating to $Fe^+(^6D)$ + L, i.e. these are adiabatic bond energies.

The $Fe^+(CO_2)$ complex differs from these other complexes in that the ground state calculated at a coupled cluster single double (triple) [CCSD(T)] atomic natural orbital (ANO) level of theory is now a sextet, with a quartet excited state lying very low in energy (0.056 eV) [7]. Our experimental value is slightly lower than the theoretical value for the sextet state (Table 5), although probably within the combined errors of theory and experiment, and agrees very well with the calculated bond energy of the quartet state. The agreement with the sextet state is certainly acceptable, especially when it is noted that the CCSD(T) theoretical value for $Co^+(CO_2)$ is also slightly higher (by 0.06 eV) than the experimental value from Lessen et al. [12]. Thus, these comparisons do not unambiguously ascertain the electronic state of the $Fe^+(CO_2)$ complex.

For the rare gas complexes, early theoretical work by Partridge and co-workers [2,4,5] on $FeAr^+$ and a more recent study by Heinemann et al. [6] on $FeAr^+$, $FeKr^+$, and $FeXe^+$ are available. For $FeAr^+$, both theoretical studies yield results within combined experimental error of the present imprecise measurement. Although the results of Partridge et al. suggest that this species has a sextet ground state, the more sophisticated analysis of Heinemann et al. makes such a conclusion ambiguous. The values obtained by Heinemann et al. are somewhat larger than the experimental values determined here but are within experimental error except for $FeXe^+$, where the disagreement is just outside the combined uncertainties. It is conceivable that these differences arise because the experimental bond energies refer to the excited sextet states of $FeKr^+$ and $FeXe^+$, which are calculated to lie 0.03 ± 0.05 and 0.10 ± 0.05 eV, respectively, higher in energy than the ground state quartet states

[6]. However, consistent values for the $FeXe^+$ bond energy (Table 3) are determined from ligand exchange reactions with $Fe^+(CO)$, $Fe^+(N_2)$, $Fe^+(H_2O)$, and $Fe^+(CO_2)$ which have been calculated to have quartet [46], quartet [17], sextet [46], and sextet [7] ground states, respectively. Thus, *spin conservation is not an obvious necessity for these reactions*. The consistent bond energies are most easily explained if all measurements correspond to the adiabatic BDE of the ground state. Thus, it is more likely that the poor agreement is attributable to shortcomings of the theoretical calculations. Although the CCSD(T) calculations of Heinemann et al. are relatively sophisticated, CCSD(T) is a single reference method. It is well known that such methods perform poorly for transition metals where near-degeneracy effects play a critical role. Furthermore, Heinemann et al. replaced 28 core electrons on Kr and 46 on Xe with a relativistic pseudopotential. This approximation, though necessary to perform the calculations at all, is quite drastic and could led to considerable error, as noted by Heinemann et al.

4.2. Comparison with literature experimental values

Ligand exchange reactions have been performed by Schwarz and co-workers to determine relative BDEs for $FeXe^+$, $Fe^+(N_2)$, $Fe^+(CO_2)$, and $Fe^+(CH_4)$ [16–18]. Although the absolute values listed in these three papers differ, this discrepancy is exclusively because different anchors were used as information in the literature evolved. Thus, values taken from Dieterle et al. [18] represent a synthesis of all thermodynamic values available in the work of Schwarz and coworkers. These are listed in Table 5 and were anchored to a value for $D_0(Fe^+–CH_4)$ measured by CID in our laboratory [21]. To make a detailed comparison to these values, it should be realized that these data come from equilibrium measurements, and hence are derived by correcting ΔG_{298} values to ΔH_0 values. Hence, we convert our 0 K thermochemistry as listed in Table 3 to 298 K enthalpies and free energies in Table 4. The latter can be compared directly with the values from Dieterle et al. [18], which are also listed in Table 4. Comparison of these data shows good agreement, within one standard deviation, as long as we use the molecular parameters for a linear $Fe^+(CO_2)$ complex. Free energies derived assuming a T-shaped complex do not agree well with the values from Dieterle et al. Thus, the correction term used by Dieterle et al. to derive the 0 K bond energy for $Fe^+(CO_2)$ appears to be in error. When the correction terms derived here are used to correct their 298 K free energy values to 0 K, we obtain the revised bond energies listed in Table 5. In all cases, these agree nicely with the present recommended values.

Further relevant information regarding this assignment comes from the spectroscopic work of Brucat and co-workers [8]. They determined that the $Co^+(CO_2)$ complex was linear, in agreement with theory [7] and our assignment here for $Fe^+(CO_2)$, and found a bond energy of 0.863 eV, which is technically a lower limit [12]. The $Ni^+(CO_2)$ complex is also strongly bound at 1.08 eV [13]. Both of these complexes correlate to metal ions in $3d^n$ ground state configurations (where $n = 8$ and 9, respectively). The comparable state for the $Fe^+(CO_2)$ system is the quartet state ($n = 7$), where the $Fe^+(^4F)$ asymptote lies 0.232 eV above the $Fe^+(^6D)$ ground state [53]. Thus, on the basis of the $Co^+(CO_2)$ bond energy, we would expect that the quartet state of $Fe^+(CO_2)$ would be bound by about $0.863 - 0.232 = 0.631$ eV. This estimate is in excellent agreement with the value determined here and our revision of the value of Dieterle et al. (Table 5), but not outside the error limits of the 0.56 ± 0.08 eV value determined previously by Schwarz and co-workers.

4.3. Efficiency of reaction

It has been pointed out that $Fe^+(N_2) + Xe \rightarrow FeXe^+ + N_2$ is driven by a favorable increase in entropy by the displacement of the dinitrogen molecule by xenon [17]. The extra rotational degrees of freedom on the product side outweigh the additional internal degrees of freedom in the $Fe^+(N_2)$ system (the $Fe^+–N_2$ bends). This result holds for all N_2/rare gas and CO_2/rare gas exchanges, assuming a linear $Fe^+(CO_2)$ complex. However, according to our thermochemistry, the only case where the endothermicity

of the ligand exchange reaction is sufficiently low that the entropy can potentially change the sign of the free energy of reaction is for the case of Xe displacing N_2. This is shown in Table 4 where it can be seen that the $T\Delta_r S_{298}$ term and $\Delta_r H_0$ terms are nearly equal and the $\Delta_r H_{298} - \Delta_r H_0$ term is small for this system. In contrast, when the exchanges involve N_2, CO_2, or methane but no rare gas, the entropy term is considerably smaller. Interestingly, the enthalpy for the $Fe^+(CO_2) + CH_4 \rightarrow Fe^+(CH_4) + CO_2$ reaction is sufficiently small that the free energy of reaction can also change sign from 0 to 298 K.

This dichotomy between endoergic and endothermic reactions is reflected by the shapes and magnitudes of the experimental cross sections. When a reaction is both endoergic and endothermic (Figs. 1, 2, 6, and 7), the cross section increases with increasing energy. When a reaction is both exoergic and exothermic, the cross section decreases monotonically with energy and the magnitude is large (Figs. 4 and 5). When a reaction is exoergic or nearly so but endothermic, the cross section decreases with energy but is much smaller than the collision cross section (Figs. 3 and 8). Apparently, the increased density of states of the products in these latter systems allows efficient product formation from thermally excited states of the reactants, the populations of which control the magnitude of the resultant cross sections at thermal energies. Thus, the observation that a ligand will displace another at room temperature (Figs. 3–5, 7, and 8) is an unreliable method of determining the exo- or endoergicity of a reaction. The efficiency of this process is an important aspect of such a determination. An example of such a misassignment is the early bracketing experiment of Schwarz and Schwarz [16] in which they concluded that $D(Fe^+–CO_2) < D(Fe^+–Xe)$, in contrast to later work [18] and the present results, Table 5.

4.4. Trends in Fe^+–L BDEs

For the rare gas series, Ar, Kr, and Xe, the Fe^+–Rg BDE increases, Table 5, following the trend of increasing polarizability [50]. The ratios of the bond energies for Fe^+–Ar, Fe^+–Kr, and Fe^+–Xe increase as $0.25 \pm 0.23 : 0.70 \pm 0.18 : 1.00$, whereas the polarizabilities for the three ligands (1.64, 2.48, and 4.02 Å^3, respectively [50]) increase as 0.41 : 0.62 : 1.00. As the polarizability of the rare gas atom increases, the rare gas distorts more when it interacts with the metal ion, increasing the binding energy. In contrast, the polarizabilities of the other three ligands considered here, N_2, CO_2, and CH_4 (1.74, 2.59, and 2.56 Å^3, respectively [50]), are comparable to Ar or Kr, but have bond energies that exceed those of the comparable rare gas by 0.3–0.4 eV. None of these ligands have dipole moments but the molecular ligands do have quadrupole moments that could enhance the bonding compared to the ion-induced dipole interaction operative for the rare gas ligands. It also seems likely that there are covalent contributions to the bonding associated with metal–ligand σ donation, π backbonding that accounts for some of this increase [17]. Additional evidence for such covalency is the observation that the CO ligand (α = 1.94 Å^3, μ_D = 0.1 D [50]) has a much stronger bond to Fe^+($D_0 = 1.59 \pm 0.08$ eV [20,22]) presumably because it is a better ligand in this respect.

Acknowledgement

This research is funded by the National Science Foundation, CHE No. 9877162.

References

[1] C.W. Bauschlicher, H. Partridge, S.R. Langhoff, J. Chem. Phys. 91 (1989) 4722.
[2] C.W. Bauschlicher, H. Partridge, S.R. Langhoff, Chem. Phys. Lett. 165 (1990) 272.
[3] C.W. Bauschlicher, H. Partridge, S.R. Langhoff, J. Phys. Chem. 96 (1992) 2475.
[4] H. Partridge, C.W. Bauschlicher, S.R. Langhoff, J. Phys. Chem. 96 (1992) 5350.
[5] H. Partridge, C.W. Bauschlicher, J. Phys. Chem. 98 (1994) 2301.
[6] C. Heinemann, J. Schwarz, W. Koch, H. Schwarz, J. Chem. Phys. 103 (1995) 4551.
[7] M. Sodupe, V. Branchadell, M. Rosi, C.W. Bauschlicher, J. Phys. Chem. A 101 (1997) 7854.
[8] D.E. Lessen, P.J. Brucat, Chem. Phys. Lett. 152 (1988) 473; J. Chem. Phys. 90 (1989) 6296; 91 (1989) 4522.
[9] D.E. Lessen, P.J. Brucat, J. Chem. Phys. 90 (1989) 6296.

[10] D.E. Lessen, P.J. Brucat, J. Chem. Phys. 91 (1989) 4522.
[11] D.E. Lessen, R.L. Asher, P.J. Brucat, Chem. Phys. Lett. 171 (1991) 380.
[12] R.L. Asher, D. Bellert, T. Buthelezi, P.J. Brucat, Chem. Phys. Lett. 227 (1994) 623; 228 (1994) 5599.
[13] R.L. Asher, D. Bellert, T. Buthelezi, G. Weerasekera, P.J. Brucat, Chem. Phys. Lett. 228 (1994) 390.
[14] P.R. Kemper, M.-T. Hsu, M.T. Bowers, J. Phys. Chem. 95 (1991) 10600.
[15] G. von Heldon, P.R. Kemper, M.T. Bowers, J. Chem. Phys. 96 (1992) 6591.
[16] J. Schwarz, H. Schwarz, Organometallics 13 (1994) 1518.
[17] J. Schwarz, C. Heinemann, H. Schwarz, J. Phys. Chem. 103 (1995) 4551.
[18] M. Dieterle, J.N. Harvey, C. Heinemann, J. Schwarz, D. Schroder, H. Schwarz, Chem. Phys. Lett. 277 (1997) 399.
[19] Our previously published transition metal thermochemistry has been reevaluated in P.B. Armentrout, B.L. Kickel, in Organometallic Ion Chemistry, B.S. Freiser (Ed.), Kluwer, Dordrecht, 1996, pp. 1–45.
[20] R.H. Schultz, K.C. Crellin, P.B. Armentrout, J. Am Chem. Soc. 113 (1991) 8590.
[21] R.H. Schultz, P.B. Armentrout, J. Phys. Chem. 97 (1993) 596.
[22] B.L. Tjelta, P.B. Armentrout, J. Phys. Chem. A 101 (1997) 2064.
[23] R.H. Schultz, P.B. Armentrout, J. Phys. Chem. 96 (1992) 1662.
[24] K.M. Ervin, P.B. Armentrout, J. Chem. Phys. 83 (1985) 166.
[25] R.H. Schultz, P.B. Armentrout, Int. J. Mass Spectrom. Ion Processes 107 (1991) 29.
[26] E. Teloy, D. Gerlich, Chem. Phys. 4 (1974) 417.
[27] D. Gerlich, Diplomarbeit, University of Freiburg, Federal Republic of Germany, 1971.
[28] F.A. Khan, D.E. Clemmer, R.H. Schultz, P.B. Armentrout, J. Chem. Phys. 97 (1993) 7978.
[29] N.F. Dalleska, K. Honma, P.B. Armentrout, J. Am. Chem. Soc. 115 (1993) 12125.
[30] N.F. Dalleska, K. Honma, L.S. Sunderlin, P.B. Armentrout, J. Am. Chem. Soc. 116 (1994) 3519.
[31] N. Aristov, P.B. Armentrout, J. Am. Chem. Soc. 108 (1986) 1806, and references therein.
[32] P.B. Armentrout, in Advances in Gas Phase Ion Chemistry, N.G. Adams, L.M. Babcock (Eds.), JAI, Greenwich, 1992, Vol.1, pp 83–119.
[33] T. Shimanouchi, Tables of Molecular Vibrational Frequencies: Consolidated Volume I, NSRDS-NBS 39, U.S. GPO, Washington, DC, 1972.
[34] T. Beyer, D.F. Swinehart, Comm. Assoc. Comput. Machines 16 (1973) 379.
[35] S.E. Stein, B.S. Rabinovitch, J. Chem. Phys. 58 (1973) 2438.
[36] S.E. Stein, B.S. Rabinovitch, Chem. Phys. Lett. 49 (1977) 183.
[37] R.G. Gilbert, S.C. Smith, Theory of Unimolecular and Recombination Reactions, Blackwell Science, Oxford, 1990.
[38] M.E. Weber, J.L. Elkind, P.B. Armentrout, J. Chem. Phys. 84 (1986) 1521.
[39] B.H. Boo, P.B. Armentrout, J. Am. Chem. Soc. 109 (1987) 3459.
[40] K.M. Ervin, P.B. Armentrout, J. Chem. Phys. 86 (1987) 2659.
[41] J.L. Elkind, P.B. Armentrout, J. Phys. Chem. 88 (1984) 5454.
[42] P.B. Armentrout, in Structure/Reactivity and Thermochemistry of Ions, P. Ausloos, S.G. Lias (Eds.), Reidel, Dordrecht, 1987, pp. 97–164.
[43] P.B. Armentrout, J. Simons, J. Am. Chem. Soc. 114 (1992) 8627.
[44] G. Herzberg, Electronic Spectra of Polyatomic Molecules, Van Nostrand Reinhold, New York, 1966.
[45] L. Capron, W.Y. Feng, C. Lifshitz, B.L. Tjelta, P. B. Armentrout, J. Phys. Chem. 100 (1996) 16571.
[46] A. Ricca, C.W. Bauschlicher, M. Rosi, J. Phys. Chem. 98 (1994) 9498.
[47] K.P. Huber, G. Herzberg, Constants of Diatomic Molecules, van Nostrand Rheinhold, New York, 1979.
[48] S.G. Lias, J.E. Bartmess, J.F. Liebman, J.L. Levin, R.D. Levin, W.G. Mallard, J. Phys. Chem. Ref. Data, Suppl. 17 (1988) 1.
[49] G. Gioumousis, D.P. Stevenson, J. Chem. Phys. 29 (1958) 292.
[50] E.W. Rothe, R.B. Bernstein, J. Chem. Phys. 316 (1959) 1619.
[51] K.M. Ervin, P.B. Armentrout, J. Chem. Phys. 80 (1984) 2978.
[52] D.G. Musaev, K. Morokuma, J. Chem. Phys. 101 (1994) 10697.
[53] C. Corliss, J. Sugar, J. Phys. Chem. Ref. Data, Suppl. 2, 14 (1985) 1.